ELSEVIER

Colloids and Surfaces
A: Physicochemical and Engineering Aspects 206 (2002) 87–104

COLLOIDS AND SURFACES A

www.elsevier.com/locate/colsurfa

Sliding drops on an inclined plane

Uwe Thiele [a,*], Kai Neuffer [a,b], Michael Bestehorn [b], Yves Pomeau [a,c], Manuel G. Velarde [a]

[a] *Instituto Pluridisciplinar, Universidad Complutense, Paseo Juan XXIII, 1, 28040 Madrid, Spain*
[b] *Lehrstuhl für Statistische Physik und Nichtlineare Dynamik, BTU-Cottbus, Erich-Weinert-Strasse 1, 03046 Cottbus, Germany*
[c] *Laboratoire de Physique Statistique de l'Ecole Normale Supérieure, associé au CNRS, 24 Rue Lhomond, 75231 Paris Cedex 05, France*

Abstract

An evolution equation for the film thickness was derived recently combining diffuse interface theory and long-wave approximation (Phys. Rev. E 62 (2000) 2480). Based on results for the structure formation in a thin liquid film on a horizontal plane, we study one-dimensional periodic drop profiles sliding down an inclined plane. The analysis of the dependence of their amplitude, velocity, advancing and receding dynamic contact angles on period and the interaction parameters reveals an universal regime of flat drops. The main properties of the flat drops do not depend on their volume. Both types of drops—the universal flat drops and the non-universal drops—are analyzed in detail, especially the dependence of their properties on inclination angle. Finally, an outlook is given on two-dimensional drops and front instabilities.

Keywords: Thin film structure and morphology; Interfacial instability; Diffuse interface theory; Sliding drops

1. Introduction

The investigation of structure formation in thin liquid films comprises many different aspects of their behavior that are important for both, the improvement of the basic understanding of the underlying physics and the applications in a wide field of areas. Two well studied problems are the rupture and dewetting of a very thin liquid film on a solid substrate and the formation of surface waves in thin films flowing down an inclined plane [1].

If a solid surface is covered by a liquid and the combination of substrate, liquid and surrounding gas is such, that the situation is energetically unfavorable (non- or partially wetting), after some transient the liquid is collected in drops on the surface, assuming that gravity is acting vertically and in downwards direction. As a result the solid–liquid and the liquid–gas interface form an equilibrium contact angle determined by the various molecular interactions. For relatively large drops the angle is given by a combination of the various interface tensions (Young–Laplace relation) [2]. However, the interface tensions only account for the 'mismatch' of the molecular inter-

* Corresponding author. Present address: Department of Physics, University of California, Berkeley, CA 94720-7300, USA. http://www.uwethiele.de.
E-mail address: thiele@mpipks-dresden.mpg.de (U. Thiele).

0927-7757/02/$ - see front matter
PII: S0927-7757(02)00082-1

actions at the interface of two semi-infinite half spaces filled with different substances. Therefore, for very small thicknesses (< 100 nm) of the thin liquid film between substrate and surrounding gas one has to correct the error made by using the bulk interface tensions by explicitly introducing distance dependent molecular interactions in the hydrodynamic equations. Normally, this is done by using an additional pressure term, the disjoining or conjoining pressure introduced first by Derjaguin [3,4]. This pressure may comprise long-range van der Waals and/or various types of short-range interaction terms [5–8].

If the liquid forms a very thin film of finite extension on the substrate because of viscosity the dynamics of retraction at the outer edges of the liquid film is very slow and the transition towards drops eventually starts at many points with spontaneous film rupture due to a surface instability, called spinodal dewetting [9], or due to nucleation at defects [10]. Lateral growth of the resulting holes yields a network of liquid rims that may decay later into small drops [11]. The process and the resulting structures are in principle well understood. For a short review see the introduction of [12] in this volume. If however, the liquid is not deposited as a thin film but already in form of a drop, it relaxes towards its equilibrium shape by spreading or retracting [1,2,13,14]. Both, the growth of a hole and the spreading of a drop involve the movement of a three phase contact line. If this line is seen as a material line its movement is made impossible by the no-slip boundary condition at the liquid–solid interface. The contact line can only move if a very thin precursor film is introduced on the 'dry' parts of the substrate or if the no-slip condition is replaced by some sort of slip condition near the contact line [2,15,16].

Independently of the behavior of a very thin film on a substrate discussed above, many groups studied the behavior of a thin liquid film flowing down an inclined plane, sometimes called 'falling films'. First experiments on falling films were performed to study the formation of surface waves [17]. Later the interest also focused on the occurrence of localized structures and their interaction [18]. Falling films and later also falling films on heated substrates were analyzed using linear stability analysis [19,20], weakly non-linear analysis [21–25] and integration of the time dependent equations [26,27]. However, all these studies focus mainly on the surface instability caused by inertia (measured by the Reynolds number). Because the molecular interactions between film and substrate are normally neglected the obtained results cannot be applied to very thin films or to drops on very thin films.

This is also the case for most works that focus on the evolution of falling sheets or ridges [28,29], i.e. the advancing edge of a fluid film or long one-dimensional drops on an inclined 'dry' substrate. As for the spreading drop a precursor film or slip at the substrate [15,30,31] helps to avoid divergence problems at the contact line, but introduces new ad-hoc parameters into the model. The additional parameters, namely the slip length or the precursor film thickness have an influence on the base state profiles and on the transverse front instability (growth rate and fastest growing wavenumber) [31–34]. Also the equilibrium and dynamic contact angles remain to be fixed independently in this kind of theory [15,35,36]. An alternative approach [37] treats either the vapor–liquid or fluid–solid interface, or both, as a separate phase whose properties differ from the bulk properties. In a study of a droplet of non wetting viscous liquid rolling down an inclined plane [38,39] it was shown that in this case the classical stress singularity at the contact line is alleviated. Recent experiments on drops on an inclined plane found stationary drops of different, angle-dependent shape that slide down the plane without changing shape [40].

Recently, the long-wave approximation for thin films [1] and a diffuse interface description for the liquid–gas interface [41] were combined to derive a film thickness equation that incorporates a disjoining pressure term [42]. There, first the vertical density profile for the liquid in a flat horizontal layer of fluid is determined taking into account the smooth but nevertheless relatively sharp density transition between fluid and gas, and the density variation close to the solid substrate. The latter variation is due to the molecular interactions and is incorporated into the calculation

through the boundary condition for the fluid density at the substrate. However, note that, the notation *interaction* is after all rather vague: the effective exponential interaction between substrate and liquid–gas interface represented by the disjoining pressure is derived from thick interface theory, but it is not obviously present as a molecular interaction in the local van der Waals equation for the density of the liquid. This difficulty, namely the difference between molecular interaction and effective interaction between mesoscale objects like interfaces and surfaces, is often overlooked in works on the topic. To account for dynamical situations the obtained density profile is then combined with the Stokes equation in the long wave approximation. The film thickness equation derived in this way has the usual form of a thin film equation with disjoining pressure [1], where the disjoining pressure now results from diffuse interface theory. This theory is fully consistent with Stokes equation of fluid mechanics and with Young–Laplace equilibrium theory in its van der Waals formulation. The structure formation in an unstable liquid film on a horizontal solid substrate was studied using this evolution equation in Ref. [43] and is reviewed and extended in this volume [12]. Based on this results a study of structure formation in a flowing film on an inclined plane was performed in Ref. [44], which is here reviewed and extended toward parameter values corresponding to a broader range of physical situations. The crucial difference to the contributions on falling films mentioned above is that here the surface instability is caused by the molecular interaction between film and substrate and not by inertia. However, the resulting structure formation results from an interplay of the molecular interactions and the viscous flow due to the inclination of the plane.

In Section 2 the evolution equation for the film thickness is discussed, the equation is non-dimensionalized by an appropriate scaling and the ordinary differential equation describing stationary surface profiles is derived. In Section 3 flat film solutions and their stability are discussed before studying the families of stationary periodic solutions in Section 4. The different family types found in Ref. [44] are shortly revised before embarking on a detailed study of the dependence of the properties of the periodic solutions on period, inclination angle, wetting properties and ratio of the strength of gravitation and molecular interaction.

Flat drops are identified as solutions with universal behavior, i.e. drops whose amplitude, velocity, and dynamic contact angles do not depend on mean film thickness. The dependence of their properties on the inclination angle is studied in Section 4.1. Finally, in Section 5 we give an outlook towards the time evolution of two-dimensional drop profiles.

In the conclusion we discuss the results in the context of other approaches and explain the relation of the study of sliding drops performed here and work on moving concentration profiles described by the convective Cahn–Hilliard equation [45].

2. Film thickness equation

We study the film evolution equation derived by Pismen and Pomeau [42] for a thin liquid film flowing down an inclined plane. For a two-dimensional geometry as sketched in Fig. 1, we have

$$\partial_t h = -\partial_x(Q(h)\{\partial_x[\gamma\,\partial_{xx}h - \partial_h f(h,a)] + \bar{\alpha}\rho g\}). \tag{1}$$

$h(x,t)$ denotes the x-dependent film thickness, $Q(h) = h^3/3\eta$ is the mobility factor arising for Poiseuille flow; ρ, γ and η are the respective density, surface tension and viscosity of the liquid, g is the gravitational acceleration and $\bar{\alpha}$ is the small inclination angle measured between the inclined

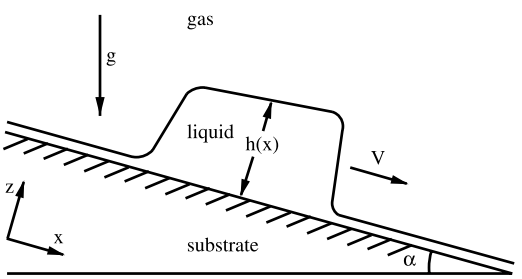

Fig. 1. Sketch of the geometry.

plane and the horizontal. x is the coordinate along the inclined plane increasing downwards. The subscripts t, x and h denote the corresponding partial derivatives. Furthermore,

$$\partial_h f(h,a) = \kappa M(h,a) + \rho g h = \frac{2\kappa}{a}\,\mathrm{e}^{-h/l}\left(1-\frac{1}{a}\,\mathrm{e}^{-h/l}\right) + \rho g h, \qquad (2)$$

is the derivative of the free energy, $f(h,a)$, and has the dimension of a pressure. $\Pi(h) = -\kappa M(h,a)$ is the disjoining pressure derived from diffuse interface theory [42], a is a small positive parameter describing the wetting properties in the regime of partial wetting, l is the length scale of the diffuse interface, and κ is the strength of the molecular interaction having the dimension of a spreading coefficient per length. Eq. (1) has the form of a mass conservation law at $\partial_t h = -\partial_x \Gamma(x,t)$, where $\Gamma(x,t)$ is the flow composed of: (i) the flow due to the gradient of the laplace or curvature pressure, $-\gamma\partial_{xx}h$; (ii) the flow due to gradients of additional pressure terms, $\partial_h f(h,a)$, (resulting from molecular interactions, $\kappa M(h,a)$, and hydrostatic pressure, $\rho g h$); and (iii) the gravitational driven flow down the inclined plane, $\bar{\alpha}\rho g$.

We introduce suitable new scales to obtain dimensionless quantities (with tilde):

$$x = \sqrt{\frac{l\gamma}{\kappa}}\,\tilde{x}, \qquad h = l\tilde{h}, \qquad t = \frac{3\eta\gamma}{\kappa^2 l}\,\tilde{t}. \qquad (3)$$

After dropping the tildes the dimensionless film evolution equation is:

$$\partial_t h = -\partial_x\{h^3[\partial_x(\partial_{xx}h - M(h,a) - Gh) + \alpha G]\}, \qquad (4)$$

$$\alpha = \bar{\alpha}\left(\frac{\gamma}{\kappa l}\right)^{1/2} \quad \text{and} \quad G = \frac{l\rho g}{\kappa}. \qquad (5)$$

For the slightly non-wetting situation, spreading coefficients are very small, implying in the diffuse interface approach that the ratio $\kappa l/\gamma$ is $O(a^2)$ with a being a small parameter [42]. Then the scale in x-direction is $O(l/a)$ and $\alpha = \bar{\alpha}/O(a)$ is not any longer a small parameter. G expresses the ratio of gravitation and molecular interactions with its value taken to be always positive in this work. Negative values would arise for a liquid film below an inclined plane that also partially wets the substrate. From here on we will only use the introduced dimensionless quantities to study the qualitative behavior of a liquid layer on an inclined plane. However, let us roughly estimate the values for G that are to be expected in real physical situations. Assuming $\kappa l/\gamma \approx a^2$ as discussed above, G can be written as $l^2/l_c^2 a^2$, where l_c, is the 'normal' capillary length $\sqrt{\gamma/\rho g}$. Taking now $l_c \approx 10^{-3}$ m, l in the nanometer range and a to lie between 10^{-4} and 0.1 gives a range for G between 10^{-2} and 10^{-10}. The main scope of this contribution is beside reviewing results obtained in Ref. [44] for relatively large G between 0.01 and 0.1 to extend the calculations toward very small G down to 10^{-7} to show, that the qualitative results regarding solution types and their behavior are mainly unchanged.

Now the remaining constant in the disjoining pressure, a, is transfered into the mobility factor Q by the transformation $\bar{h} = h + \ln a$ to facilitate the comparison with results obtained for pattern formation on a horizontal substrate [43,12].

After dropping the bar, in Eq. (1) becomes

$$\partial_t h = -\partial_x\{Q(h,a)[\partial_x(\partial_{xx}h - \partial_h f(h)) + \alpha G]\}. \qquad (6)$$

with the mobility factor $Q(h,a) = (h - \ln a)^3$. The derivative of the free energy now only contains the parameter G:

$$\partial_h f(h) = 2\mathrm{e}^{-h}(1-\mathrm{e}^{-h}) + Gh. \qquad (7)$$

To study stationary solutions of Eq. (6), i.e. film thickness profiles, $h(x,\mathrm{t})$, that move with a constant dimensionless velocity, v, we write Eq. (6) in the comoving coordinate system $x_{co} = x - vt$, implying $\partial_t h = -v\partial_x h$, when setting the time derivative in the comoving system to zero. Then an integration with respect to x gives,

$$0 = Q(h,a)(\partial_{xxx}h - f_{hh}\,\partial_x h) + \alpha G Q(h,a) - vh + C_0. \qquad (8)$$

C_0 is a constant of integration that here, in contrast to the reflection symmetric problem on a

horizontal plane [12], cannot be set to zero. C_0 can be identified as the flow in the comoving system. $C_0 \neq 0$ implies that a second integration is not possible. We choose

$$C_0 = -(\Gamma_0 - \upsilon h_0) = -Q(h_0, a)\alpha G + \upsilon h_0, \qquad (9)$$

to introduce a flat film or homogeneous solution of thickness h_0 in a natural way. The corresponding flow in the laboratory system, constant with respect to x, is $\Gamma_0 = -Q(h_0, a)\alpha G$.

3. Flat film solutions and their linear stability

Beside the flat film solution given by the choice of h_0 other film thicknesses, h_i, may exist that yield the same flow in the comoving frame, i.e. that are solutions of Eq. (8) with identical C_0. They correspond to additional fixed points (beside h_0) of Eq. (8), if seen as a dynamical system. Given the flow Γ_0 by prescribing h_0, there exist two such solutions for flat film thicknesses:

$$h_{1/2} = (h_0 - \ln a)\left(-\frac{1}{2} \pm \sqrt{\frac{\upsilon}{G\alpha(h_0 - \ln a)^2} - \frac{3}{4}}\right) + \ln a. \qquad (10)$$

The physical film thickness $h - \ln a$ has to be positive. Thus only the positive sign in Eq. (10) can give a physically meaningful result. Taking this choice a second flat film solution exists for $\upsilon/G\alpha(h_0 - \ln a)^2 > 1$. It corresponds to the so called conjugate solution discussed also in falling film problems as, for instance, in Ref. [46].

For $\upsilon/G\alpha(h_0 - \ln a)^2 > 3$ the second film thickness is larger than the imposed one, $h_0 - \ln a$. Note, that the second flat film thickness does not directly depend on the molecular interaction $M(h)$. However, it is known that for the limiting case $\alpha = 0$ the molecular interaction selects an upper and an lower plateau thickness (i.e. the fixed points) and therefore has also to determine the behavior for $\alpha \to 0$ as will be discussed in more detail below in Section 4.1. Note, that Eq. (10) does not serve to calculate the fixed points because the velocity, υ, is not an independent variable, but has to be determined together with the solution profiles.

The linear stability of the flat film solutions is determined by using the ansatz $h(x) = h_0 + \varepsilon\exp(\beta t + ikx)$ to linearize the time dependent Eq. (6) yielding the dispersion relation:

$$\beta = -(h_0 - \ln a)^3 k^2 (k^2 + f_{hh}|_{h_0}) - i3\alpha G k (h_0 - \ln a)^2. \qquad (11)$$

The growth rate of the harmonic mode with wavenumber k is given by the real part of $\beta(k)$, whereas its imaginary part determines the downwards phase velocity of the mode to be $\upsilon = -\mathrm{Im}\,\beta/k = 3\alpha G(h_0 - \ln a)^2$. This corresponds to the fluid velocity at the surface of the unperturbed flat film.

The onset of the instability occurs with $k = 0$ for $\mathrm{Re}\,\beta = 0$. Using Eq. (7) yields linear instability for,

$$f_{hh}(h_0) = -2\mathrm{e}^{-h_0}(1 - 2\mathrm{e}^{-h_0}) + G < 0, \qquad (12)$$

i.e. for the intermediate thickness range,

$$h_- < h_0 < h_+ \qquad (13)$$

where,

$$h_\pm = -\ln\left[\frac{1}{2}\left(\frac{1}{2} \mp \sqrt{\frac{1}{4} - G}\right)\right]. \qquad (14)$$

For $G \ll 1$ one finds $h_- \approx -\ln(G/2)$ and $h_+ \approx \ln 2 + G$. There is a critical point at ($G_c = 1/4$, $h_c, = \ln 4$) where the lower and the upper linear instability border meet. For $G > G_c$, flat films are always linearly stable.

Given a film thickness in the linearly unstable range, the critical wavenumber, k_c, as determined by $\mathrm{Re}\,\beta = 0$, is $k_c = \sqrt{-f_{hh}(h_0)}$, whereas the fastest growing mode has the wavenumber $k_m = k_c/\sqrt{2}$ and the growth rate, $\beta_m = (h_0 - \ln a)^3 f_{hh}(h_0)^2/4$. Note, that the stability of flat film solutions does not at all depend on the dynamical aspect of the problem (inclination and velocity), but only on the molecular interactions, $f_{hh}(h)$. The stability condition is exactly as for a flat film on a horizontal substrate [12,43].

4. Periodic solutions

A linearly unstable flat film will start to evolve in time resulting in the rupture of the film or—if the evolution saturates—in a stationary film profile of finite amplitude. The stationary film profiles have to be solutions of Eq. (8) and can be found using continuation methods [47] already applied in the case of structure formation on the horizontal plane ([12] in this volume). Denoting the stationary solutions obtained in this way by $h_0(x)$ their linear stability is calculated using the ansatz $h(x) = h_0(x) + \varepsilon h_1(x)\,\mathrm{e}^{\beta t}$ in Eq. (6). Linearizing in ε gives after transforming into the comoving frame an eigenvalue problem for the growth rate, β, and disturbance, $h_1(x)$:

$$\begin{aligned}\beta h_1 = {} & \{[3q^2(h_{0x} f_{hh} - h_{0xxx})]_x + (q^3 h_{0x} f_{hhh})_x\} h_1 \\ & + [2q^3 h_{0x} f_{hhh} + 3q^2(2h_{0x} f_{hh} - h_{0xxx})] h_{1x} \\ & + q^3 f_{hh} h_{1xx} - 3q^2 h_{0x} h_{1xxx} - q^3 h_{1xxxx} \\ & - (3\alpha G q^2 h_1)_x + v h_{1x}, \end{aligned} \tag{15}$$

where $q = h_0(x) - \ln a$ and all derivatives of f are functions of the stationary profile $h_0(x)$. For details of the numerical methods, see Ref. [44]. Here, we study the linear stability of the periodic solutions taking one period of the solution as the unit of the stability analysis, i.e. the stability to small disturbances when the period is fixed. The solutions may also be unstable with respect to coarsening as in the case on the horizontal plane [43], but this is not investigated here.

First, we study periodic solutions in their dependence on period at fixed inclination angle, α, and interaction parameters, G and a. To do this we start from small amplitude stationary solutions that have the form $h(x) = h_0 + \varepsilon\,\mathrm{e}^{ikx}$ as can be seen by linearizing Eq. (8). The resulting condition $0 = k^3 + f_{hh}(h_0)k - i(3\alpha G k(h_0 - \ln a)^2 - vk)$ determines the wave number and the velocity to be $k = k_c = \sqrt{-f_{hh}(h_0)}$ and $v = 3\alpha G(h_0 - \ln a)^2$, respectively. The small amplitude stationary solutions correspond to the neutrally stable modes obtained in the linear stability analysis in Section 3 and in consequence exist only in the linearly unstable film thickness range.

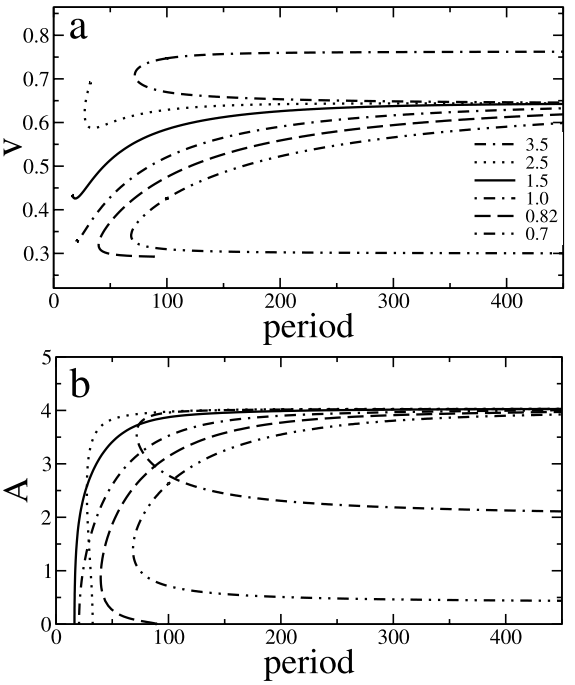

Fig. 2. Characterization of stationary periodic solutions for relatively large G. Shown are the dependencies of: (a) the velocity, v, on period; and of (b) the amplitude on period for different mean film thicknesses, $\bar{h}$, as given in the legend of (a). $G = 0.1$, $\alpha = 0.1$ and $a = 0.1$.

Solution families are continued through the parameter space starting at these stationary solutions. Fixing, for instance, $\bar{h}$, G and a, solutions with different periods are obtained. Depending on mean film thickness, $\bar{h}$, families with qualitatively different behavior are found, as shown for a relatively large G in Fig. 2(a) (velocity-period dependence) and Fig. 2(b) (amplitude-period dependence). We distinguish the following family types (listed with increasing mean film thickness).

1. For very small $\bar{h}$ only the trivial solution $h(x) = h_0$ exists.
2. Two branches exist, both continuing towards $L \to \infty$. This implies the existence of two solutions with different velocity, v, and amplitude, A, for every period larger than a minimal period. Both branches show a monotonic dependence of v and A on period, L. The small-amplitude branch consists of linearly unstable solutions and the large-amplitude branch of linearly stable ones (example: $\bar{h} = 0.7$).

3. Two branches exist, but only the branch with larger velocity continues towards $L \to \infty$. It contains the linearly stable solutions, whereas the terminating branch consist of linearly unstable solutions. Both branches show a monotonic dependence of v on L. Considering the period as a bifurcation parameter, the endpoint of the terminating branch corresponds to the locus of a subcritical bifurcation from uniform solutions to solutions oscillating in space (example: $\bar{h} = 0.82$).
4. One, linearly stable branch exists continuing towards $L \to \infty$. v and A increase monotonously with L. The endpoint of the branch corresponds to the locus of a supercritical bifurcation ($\bar{h} = 1.0$).
5. One, linearly stable branch exists continuing towards $L \to \infty$, A increases monotonously but v depends non-monotonically on period (supercritical bifurcation, example: $\bar{h} = 1.5$).
6. Two branches exist. The low velocity branch is linearly stable, continues towards $L \to \infty$ and its velocity depends non-monotonically on period. The other branch terminates at finite period, is linearly unstable and shows a monotonic dependence of v on L. (subcritical bifurcation, example: $\bar{h} = 2.5$).
7. As 2, the only difference is that the branch with lower velocity corresponds to larger amplitude (example: $\bar{h} = 3.5$).
8. For very large $\bar{h}$ the only solution is the trivial $h(x) = h_0$.

All the families described up to now resemble families of profiles found on the horizontal substrate, that are here varied by the inclination of the plane. They are not any more reflection symmetric with respect to the extrema of the profiles and move with a certain velocity. The linearly unstable branches represent nucleation solutions as for $\alpha = 0$ [43]. This was shown by direct numerical integration of Eq. (6) in Ref. [44]. The nucleation solutions give the critical disturbance for linearly stable but not absolutely stable (i.e. metastable) situations as flat films outside the linearly unstable thickness range or linearly unstable flat films with an imposed period smaller than the smallest linearly unstable wavelength. At constant shape, disturbances with smaller amplitude than the critical disturbance will relax towards the flat film, whereas an amplitude larger than critical leads to growth of the disturbance. The system will then reach the solution on the other, the stable branch.

From Fig. 2 one finds that one branch of every family converges to a line common to all families. This implies a certain 'universality' of the solutions on this line because their velocity and amplitude are independent of the mean film thickness. The convergence to the common line occurs at lower period for large mean film thickness than for small film thickness. Also the film profile converges to a common shape: a flat drop with an upper plateau of thickness, h_u, sitting on a very thin (precursor) film of thickness h_d. At the downstream front of the drop a capillary ridge forms. For the flat drops only the length of the upper plateau depends on the mean film thickness.

The phenomenology or qualitative behavior of the solutions is for G smaller then the critical value at $G_c = 1/4$ nearly independent of G. This made possible to discuss in Ref. [44] all the occurring processes for a relatively large G between 0.05 and 0.2. However, physically realistic values for G are much smaller implying a separation of the length scales for the thicknesses of the upper and lower plateau, i.e. of the precursor film thickness and drop height. For small α the thicknesses of the upper and lower plateau can be estimated to be of order $\sqrt{1/G}$ and $\sqrt{G}$, respectively, implying an order $1/G$ difference between the two plateau thicknesses. In the remaining part of this work we extend the results of Ref. [44] towards very small, more realistic values of G between 10^{-4} and 10^{-7}. Thereby, it is determined whether in the future it will be possible to describe experimental results with the numerical methods used here.

Fig. 3 gives the equivalence of a part of Fig. 2 for $G = 10^{-5}$ and Fig. 4 shows the corresponding advancing and receding contact angles defined as the absolute values of the slope of the profile at the respective inflection points. For small periods they increase strongly from their value for flat films that is zero. At larger periods the advancing angle increases slowly with period, whereas the receding angle decreases. At a period of $L = 10^6$

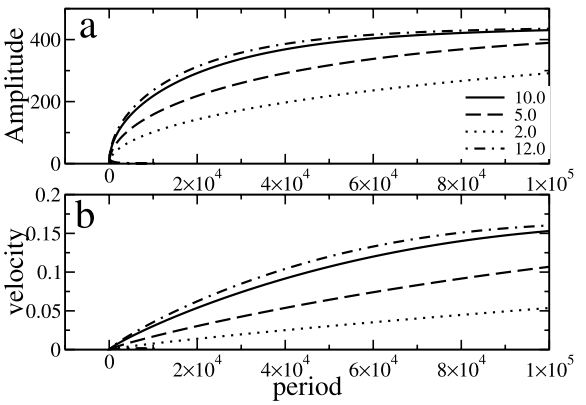

Fig. 3. Characterization of stationary periodic solutions. Shown is the dependence of: (a) the amplitude, A; and (b) the velocity, v, on period, L, for different mean film thicknesses, $\bar{h}$ (given in the legend) for $G = 10^{-5}$, $\alpha = 0.2$ and $a = 0.1$.

some of the curves in Fig. 2 have already converged onto the common line, but for the smaller mean film thicknesses still larger periods are necessary. The change of the drop profiles with increasing period can be seen for $\bar{h} = 10$ in Fig. 5(a and b). For relatively small periods the drops keep their shape, only their height and in consequence their velocity (Fig. 3(b)) increase with period. Then, at about $L = 50\,000$ the shape starts to change: the height increases only slowly but the drop starts to develop a hunchback that prolongs

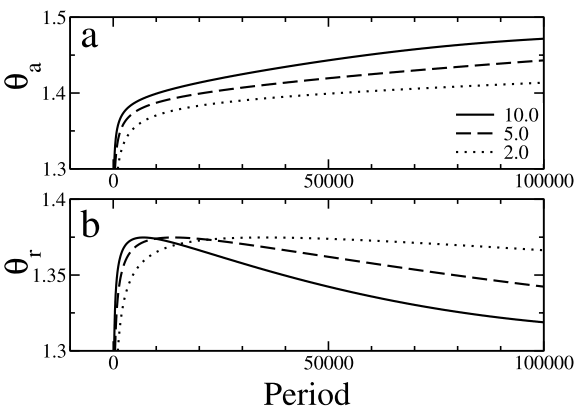

Fig. 4. Characterization of stationary periodic solutions. Shown is the dependence of: (a) the advancing dynamic contact angle, θ_a; and (b) the receding dynamic contact angle, θ_r, on period, L, for different mean film thicknesses, $\bar{h}$ (given in the legend) for $G = 10^{-5}$, $\alpha = 0.2$ and $a = 0.1$.

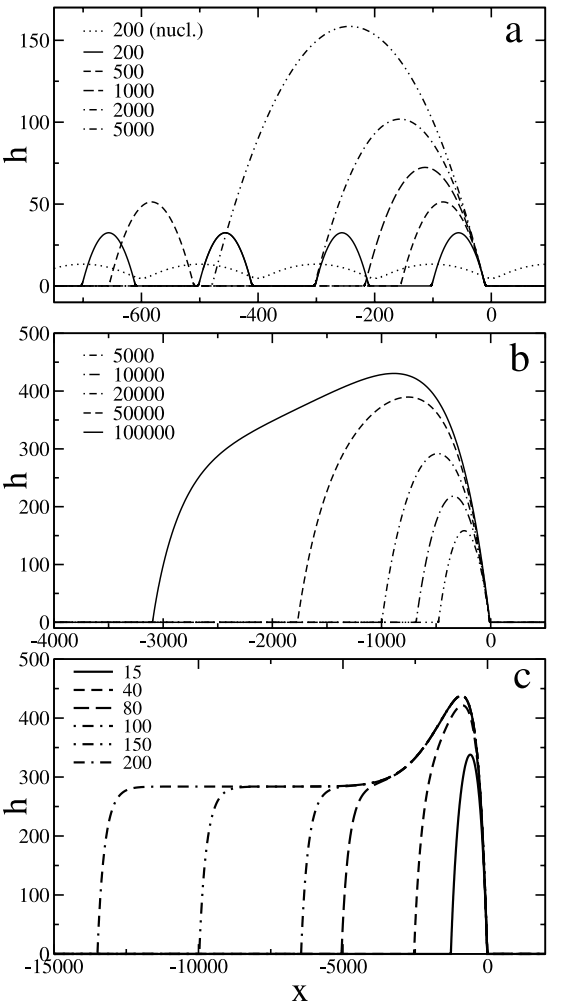

Fig. 5. Profiles for different period, L, for mean film thickness $\bar{h} = 10$. $G = 10^{-5}$, $\alpha = 0.2$ and $a = 0.1$. Part (a) and (b) show different ranges of the period as given in the legend. The emergence of flat drops is shown in part (c), where the period is fixed at $L = 100\,000$ and the mean film thickness is increased (values given in legend).

with increasing period. To see this process more clearly the period is fixed at $L = 10^6$ and more liquid volume is fed into the system by increasing the mean film thickness as shown in Fig. 5(c). When the profiles are on the common branch, feeding more liquid or prolonging the period only changes the length of the upper plateau, whereas the shape and height of the capillary ridge and the back front remain unchanged.

To underline the resemblance of the behavior for small and relatively large G in Fig. 6, a zoom of Fig. 3 is plotted showing the existence of branches of nucleation solutions, non-monotonic dependence of velocity on period and, consequently, the transition between family types (1–8) as described above (the figure only shows the transition between families (3) and (4). Although, we will not dwell further on this subject here, take note, that beside the solution branches having direct equivalents in the horizontal case, $\alpha = 0$ [12,43], also new surface wave branches appear for certain film thicknesses that are intrinsic features of the flowing film. In [44] this type of solutions is discussed in connection with a dynamical wetting transition with hysteresis occurring when changing the inclination. Here, we show the occurrence of the new branch in Fig. 7, an even more detailed zoom of Fig. 3 for a small range of film thicknesses. There it can be seen how the nucleation branches shown in Fig. 6 bulge out giving rise to an additional branch consisting of linearly stable surface waves.

Now, we study the influence of the interaction parameters describing the wetting properties, a, and the ratio of gravitation and molecular interaction, G. To this purpose again the dependences of the properties of the profiles on period are calculated, but now comparing different parameter values of a or G. Fig. 8(a and b), Fig. 9(a and b) show the respective change of amplitude, velocity, advancing and receding contact angle with

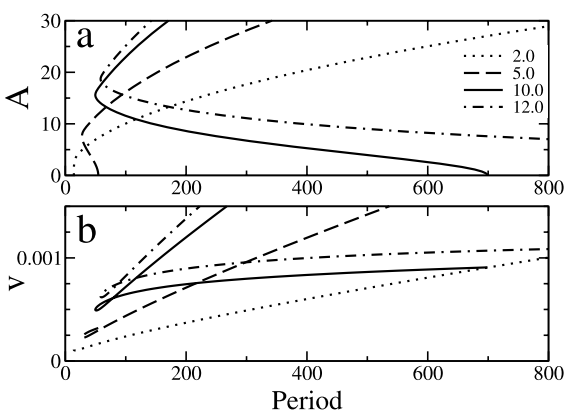

Fig. 6. Zoom of Fig. 3 for small amplitudes.

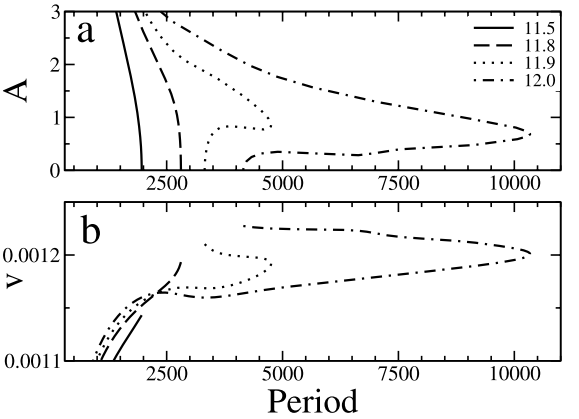

Fig. 7. Strong zoom of Fig. 3 for small amplitudes showing the solution branch of linearly stable, non-linear surface waves that have no counterpart for $\alpha = 0$.

period for different a. The curves for different G are shown in Fig. 10(a and b), Fig. 11(a and b), respectively. The wetting properties in the studied range of small partial wettability measured by a do not have an influence on the amplitude of the profiles (Fig. 8(a)), but influence both, velocity and contact angles. The latter can be easily understood remembering that in the used scaling a remains only in the mobility factor $Q(h, a) = h - \ln a$ and that the performed shift in h (Section 2) implies the existence of a physical precursor film of at least $(-\ln a)$ thickness facilitating the move-

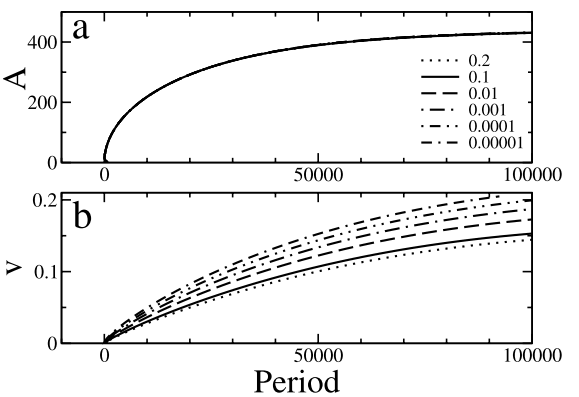

Fig. 8. Dependence of the stationary periodic solutions on the parameter a. Shown is the change of: (a) the amplitude, A; and (b) the velocity, v with period, L, for different a as given in the legend for $\bar{h} = 10.0$, $G = 10^{-5}$ and $\alpha = 0.2$.

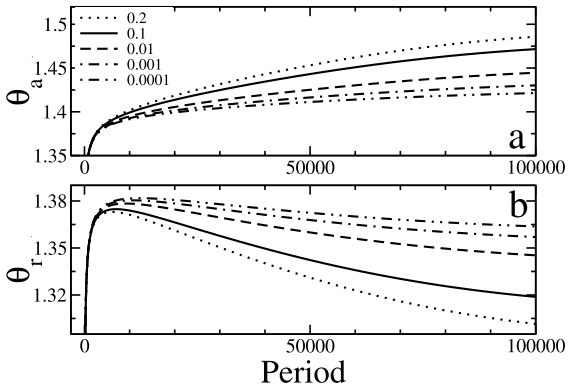

Fig. 9. Dependence of: (a) the advancing dynamic contact angle, θ_r; and (b) the receding dynamic contact angle, θ_a, on period, L, for different parameter a (given in the legend) for $\bar{h} = 10.0$, $G = 10^{-5}$ and $\alpha = 0.2$.

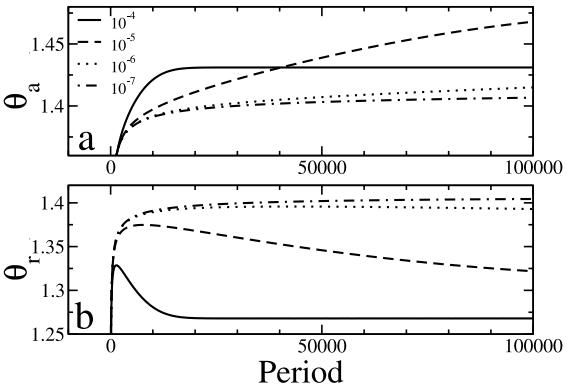

Fig. 11. Dependence of: (a) the advancing dynamic contact angle, θ_a; and (b) the receding dynamic contact angle,θ_r on period, L, for different parameter G (given in the legend) for $\bar{h} = 10.0$, $\alpha = 0.2$ and $a = 0.1$.

ment of the profiles. Fig. 9 shows that in more wettable situations (smaller a) the advancing front of the drop is less steep, whereas the back front flattens with decreasing wettability.

The ratio of gravitation and molecular interaction, G, influences crucially the dependence of all profile properties on period (Figs. 10 and 11). G has a strong impact on both, the plateau thicknesses as discussed above for the limit $\alpha \to 0$ and the driving force (last term of Eq. (6)). The smaller G the larger becomes the upper plateau thickness implying a slower convergence towards the universal flat drop solutions. The curves for $G = 10^{-4}$ have already converged at $L = 20\,000$, whereas the curve for $G = 10^{-6}$ and identical mean film thickness shows no sign of convergence even at $L = 100\,000$. Take note, that the velocity is not determined by the amplitude, i.e. it is not larger for larger amplitude but smaller G as one could expect giving the mobility factor to much importance. It seems to be only determined by the driving force that is proportional to G. However, the behavior of the dynamic contact angles (Fig. 11) is less clear. Taking only the already converged curves for $G = 10^{-4}$ and 10^{-5} into account, both angles seem to increase with decreasing G.

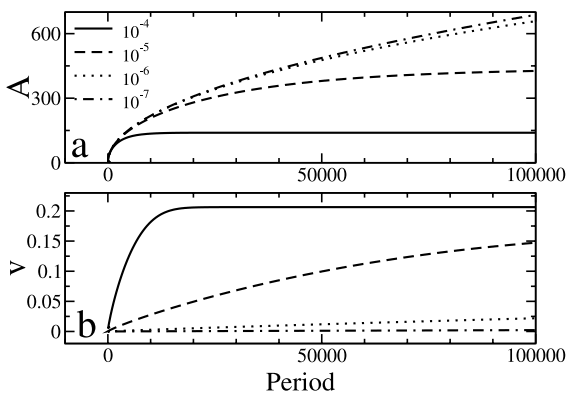

Fig. 10. Dependence of the stationary periodic solutions on the parameter G. Shown are: (a) the amplitude, A; and (b) the velocity, v as a function of the period, L, for different G as given in the legend for $\bar{h} = 0.9$, $\alpha = 0.2$and $a = 0.1$.

4.1. Dependence on inclination angle

The dependence of the properties of the flat drops on the system parameters was already studied for relatively large G [44]. There the velocity increases monotonously with α and the flat drop becomes thinner by decreasing its upper plateau thickness and increasing the lower plateau or precursor film thickness. The relative height of the capillary ridge as compared to the upper plateau thickness increases with increasing inclination. For larger inclination angles, i.e. larger velocities of the drop, secondary oscillations or 'wiggles' evolve behind the capillary ridge and in the precursor film in front of the drop.

In the limit α, $v \to 0$ for $G \ll 1$ the slope of the function $v(\alpha)$ at $\alpha = 0$ can be estimated because the plateau thicknesses have to converge to the values obtained for a drop on a non-inclined plane ($\alpha = 0$) [43]. These depend only on the properties of the free energy $f(h)$, and are for $G \ll 1$

$$h^{\mathrm{d}} = \sqrt{G/2} + \frac{3}{8} G + O(G^{3/2}) \quad \text{and}$$

$$h^{\mathrm{u}} = \sqrt{2/G} - \frac{\sqrt{2}}{16} \sqrt{G} + \frac{21}{128} G + O(G^{3/2}). \qquad (16)$$

Inserting relations Eq. (16) in the equation determining the flat film thicknesses Eq. (10), gives the condition

$$\left.\frac{v}{\alpha}\right|_{\alpha \to 0} \quad \text{tending to}$$

$$2 - 3\sqrt{2G} \ln a + \left(\frac{3}{4} + 3(\ln a)^2\right) G + O(G^{3/2}). \qquad (17)$$

This was shown to be a good estimation for the slope of the curve $v(\alpha)$ at $\alpha = 0$ [43].

As described above, fixing the period, the ratio of the length of the upper and the lower plateau is determined by the given liquid volume imposing limits for the existence of the flat drops. They cannot exist: (i) if there is not enough matter in the system to form it including the capillary ridge at its front; and (ii) if there is to much matter causing the downstream end of the drop to approach the upstream end of its predecessor. In consequence, the ends start to interact transforming the profile into a moving hole in an otherwise flat film or into small non-linear waves on an otherwise flat film. In other words, when the upper plateau thickness approaches the mean film thickness the flat drops cannot longer exist and the solution families have to depart from the universal branch as shown in Fig. 12 for relatively large G. With decreasing $\bar{h}$ the point of departure shifts towards larger inclination angles. The properties of the non-universal solutions depend strongly on the mean film thickness (further discussed in [43]). The S-shaped curve for the dependency of velocity on inclination angle for some $\bar{h}$ in Fig. 12(a) implies the existence of two linearly stable branches that are separated by an linearly unstable branch acting as nucleation solution: it has to be overcome from either side in order to jump to the other branch. This has two important effects: (I) an apparent stability of the flat film; and (II) the existence of a dynamic wetting transition with hysteresis.

(I) Because the surface waves on the large-velocity stable branch have very small amplitudes (Fig. 12(b)) they can easily be missed in an experiment that concentrates on drop formation.

(II) The existence of two linearly stable branches between two inclination angles, α_{d} and α_{u}, gives rise to hysteresis: changing α the system jumps between the linearly stable branches: from the large to the small amplitude branch at α_{u} and from the small to the large amplitude branch at α_{d}. The transition between the two branches may be called a *dynamical wetting transition with hysteresis*.

Concentrating again on small G we discuss as an example the dependence of the drop properties on inclination angle for different mean film thick-

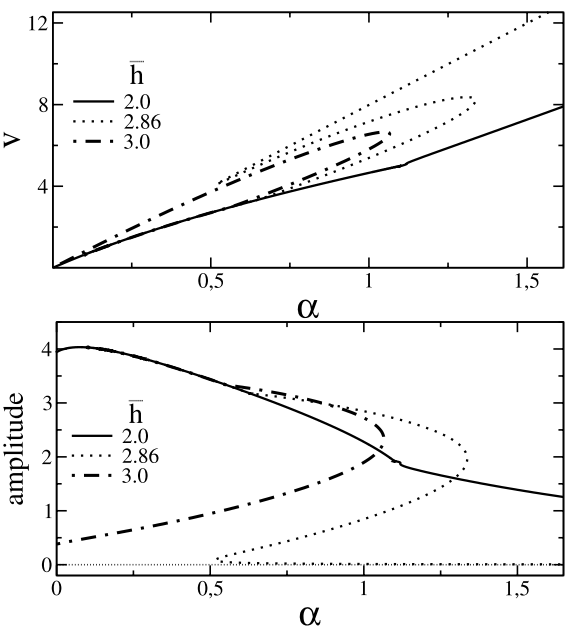

Fig. 12. The dependence of: (a) velocity, v; and (b) amplitude, A, on inclination angle, α, for different mean film thicknesses as given in the legend. $a = 0.1$, $G = 0.1$ and $L = 2000$.

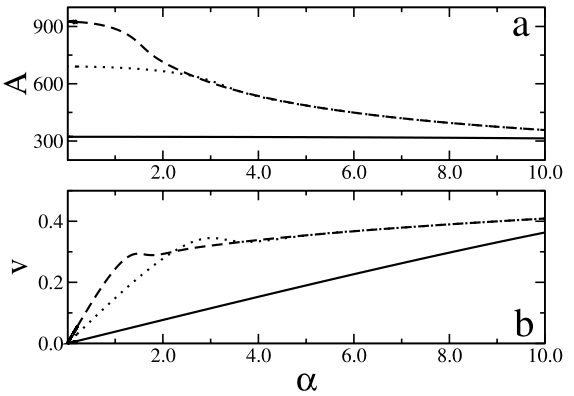

Fig. 13. The dependence of: (a) amplitude, A; and (b) velocity, v, on inclination angle, α, for different mean film thickness $\bar{h}$ as given in the legend. $G = 10^{-5}$, $a = 0.001$ and $L = 20\,000$.

nesses, but fixing $G = 10^{-5}$, $a = 0.001$ and the period $L = 20\,000$. Fig. 13(a and b), Fig. 14(a and b) show the respective dependences of amplitude, velocity, advancing and receding contact angle on inclination angle. Some profiles for different α are shown in Fig. 15. All plots show the two clearly distinguishable regimes of non-universal drops at small α and universal flat drops at larger α. The inclination angle where the transition occurs depends strongly on mean film thickness. For $\bar{h} = 10$ it is not yet reached at $\alpha = 10$. The velocity depends in both regimes linearly on α. However, the slope v/α is larger for the non-universal drops

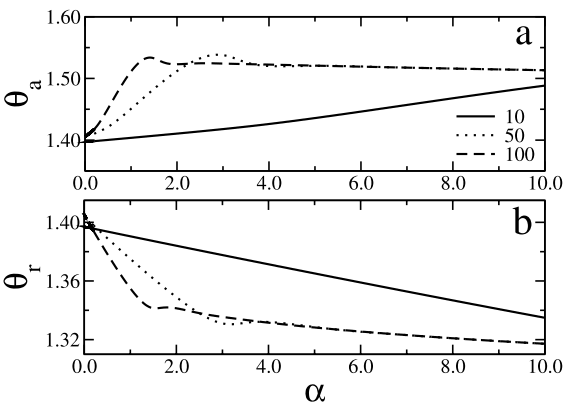

Fig. 14. The dependence of: (a) the advancing dynamic contact angle, θ_a; and (b) the receding dynamic contact angle, θ_r, on inclination angle, α, for different mean film thickness $\bar{h}$ as given in the legend. $G = 10^{-5}$, $a = 0.001$ and $L = 20\,000$.

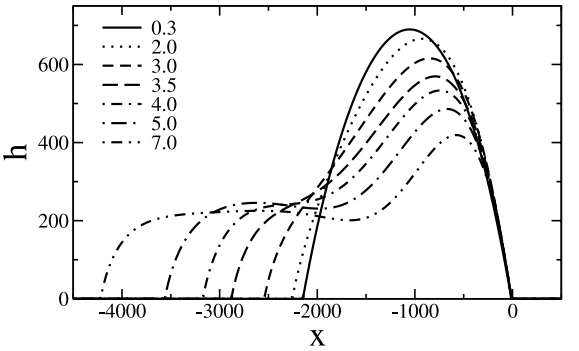

Fig. 15. Drop profiles for different inclination angle, α, as given in the legend for mean film thickness $\bar{h} = 50$. $G = 10^{-5}$, $a = 0.001$ and $L = 20\,000$.

than for the flat drops. For the non-universal drops it decreases with decreasing mean film thickness due to the lower mobility of smaller drops. The dynamic contact angles show a very interesting behavior (Fig. 14). The receding angle decreases nearly linearly in both regimes with α (smaller slope θ_r/α for the flat drops), but the advancing angle increases with α for non-universal drops and decreases slowly and linearly for the flat drops. This implies the counter intuitive decrease of the advancing angle with increasing velocity in the flat drop regime as can be seen for the larger velocities in Fig. 16. A non-monotonic dependence of the advancing angle on velocity was already noted in Ref. [44]. Take note, that in the transition region between non-universal and universal drops the overshooting of the velocity (Fig. 13) and the advancing contact angle (Fig. 14) over the respective straight lines for the flat drops results in a dependence of θ_a on v that is not one to one as shown in Fig. 16.

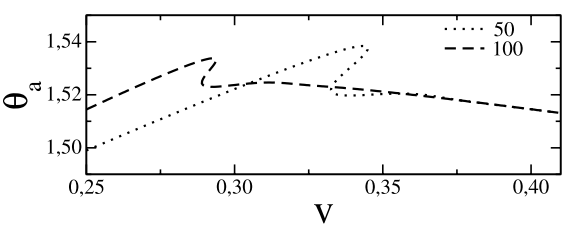

Fig. 16. The dependence of the advancing dynamic contact angle, θ_a on velocity, v. For mean film thicknesses, $\bar{h}$, as given in the legend. $G = 10^{-5}$, $a = 0.001$ and $L = 20\,000$.

In the future, the results obtained here for one-dimensional non-universal and flat drops have to be compared to results for two spatial dimensions. In the following Section 5, we give a short outlook on the numerical techniques that have to be used in this case and show some first results.

5. Two-dimensional outlook

For the first calculations in two spatial dimensions we focused our interest on the evolution of different initial states on an inclined plane. We discuss a liquid layer on a plane that is inclined in x-direction as before. The two-dimensional version of Eq. (6) reads now for $h = h(x, y, t)$:

$$\partial_t h = -\nabla\{(h - \ln a)^3[\nabla(\Delta h - \partial_h f(h)) + \alpha \boldsymbol{G}\boldsymbol{e}_x]\}, \tag{18}$$

with $\boldsymbol{e}_x$ being the unit vector in x-direction. To solve Eq. (18) numerically, the time derivative has to be discretized, in the simplest case by an Euler-forward scheme. Space can be discretized by finite differences. A fully explicit time scheme, however, would lead to severe stability restrictions on the time step, ∂_t, since on the l.h.s of Eq. (18) one has terms of the orders

$$h^3\Delta h \quad \text{and} \quad h^3\Delta^2 h,$$

whose absolute values increase rapidly with h. Therefore, it is recommended to take as many terms of this kind as possible implicitly. This can be done by introducing the mean film thickness

$$\bar{h} = \int_V \mathrm{d}x\ \mathrm{d}y\ h,$$

which is a conserved quantity and can be considered as a control parameter. Using the transformation,

$$u(x, y, t) = h(x, y, t) - \bar{h},$$

one can write Eq. (18) as,

$$\partial_t u = D(\bar{h})\ \Delta u - \bar{h}^3\ \Delta^2 u + F_{\mathrm{NL}}(u, \nabla u, \ldots) \tag{19}$$

where the 'diffusion coefficient' D turns out to be,

$$D(\bar{h}) = \bar{h}^3\left(-\frac{2}{a}\,\mathrm{e}^{-\bar{h}} + \frac{4}{a^2}\,\mathrm{e}^{-2\bar{h}} + G\right),$$

and F_{NL} denotes a non-linear function of u and its spatial derivatives up to fourth order. The first two terms in Eq. (19) are linear and can be taken implicitly, leading to the scheme

$$L(\Delta)\,u(x, y, t + \delta t) = \frac{u(x, y, t)}{\delta t} + F_{\mathrm{NL}}(t) = \Phi(x, y, t), \tag{20}$$

with the linear differential operator,

$$L(\Delta) = \frac{1}{\delta t} - D(\bar{h})\Delta + \bar{h}^3\Delta^2 \tag{21}$$

At each time step, L has to be inverted which can be done most easily in Fourier space:

$$\tilde{u}(k_x, k_y, t + \delta t) = \frac{1}{L(-k^2)}\,\tilde{\Phi}(k_x, k_y, t) \tag{22}$$

where $\tilde{u}$ and $\tilde{\Phi}$ denote the Fourier transform. The non-linearities are treated explicitly. To avoid time consuming convolution sums they are computed in real space (pseudo-spectral method). The two Fourier transforms needed at each step are done by a standard FFT routine.

The code is implemented on an alpha-workstation and allows there for a spatial resolution up to 1048×1048 mesh points. Due to the semi-implicit time integration, the time step can be fixed at values of order one. This allows computations for rather large domains in a reasonable time (some hours). For all runs we use fixed parameters $G = 0.2$ and $a = 0.1$ but different initial conditions.

1. Deformation and separation of drops. We take three drops with different size as initial pattern. Feeling the tangential component of gravity, the drops move and change their form to long ovals. Later-on cusps are formed at their trailing ends for not too large values of α. For larger values, the cusps get sharper and small drops are pinched off (Fig. 17). This is clearly a feature that lies outside the range of a one-dimensional model. The speed of the drops increases with their size as in the one-dimensional case. On smaller drops the cusps are generated faster and the separation of secondary drops is seen earlier.

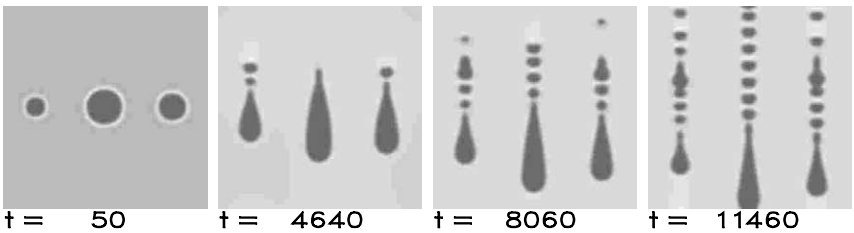

Fig. 17. Time series found by numerical integration of Eq. (18). The layer is inclined in the vertical direction in the figure. The film falls downwards. Initial condition are three drops of different volume. After inclining to $\alpha = 0.2$ larger drops travel faster. The inclination angle shown is large enough to observe secondary drops pinch off from the cusp of the primary drops. We fixed $\bar{h} = 3.2$ in the metastable region to avoid instability of the flat domains. 256×256 points. $G = 0.2$, $a = 0.1$ and domain size equal to 950.

2. Formation of rivulets. Starting the numerical integration with an initial pattern of 200 randomly distributed small drops, the evolution shown in Fig. 18 takes place. Drops coalesce to narrow rivulets meandering downwards. At the trailing end of a rivulet, drops are pinched off from time to time and are left behind. In contrast to the one-dimensional situation, stationary patterns were not found.
3. Fronts and fingers. Next we study the instability of a one-dimensional flat drop that is continued homogeneously in the transversal y-direction, i.e. of a liquid ridge that is translation invariant in y-direction. For $\alpha = 0.2$ the advancing front of the ridge gets transversely unstable to periodic disturbances (Fig. 19). From these disturbances, more or less equally spaced fingers grow. The transverse wave number of the finger pattern in Fig. 19 is $k \approx 0.05$, which is about half of the critical wave number of the flat film instability calculated in Section 3. Qualitatively, the same picture was obtained in experiments with falling films of silicone oil or glycerine [48,28], and numerically in a very recent work with a different disjoining pressure [49].

Finally, Fig. 20 shows an evolution starting from a similar initial condition as in Eq. (3), where both fronts, the advancing *and* the receding one, are unstable to transverse periodic disturbances. It is interesting to see that the wavelengths of the growing inhomogeneities are different for the two fronts. Growth rate as well as wavelength depend also on the inclination of the plane. Finally, rivulets arise as obtained in Fig. 18.

6. Conclusion

We have revised and extended the analysis of the evolution of a thin liquid film flowing down an inclined plane. The model of interaction with the substrate used is based on a disjoining pressure arising in a diffuse interface theory coupling van der Waals equations and thin film hydrodynamics [42]. We have studied flat film solutions and their linear stability and have found that although the thickness of the flat film solutions depends on velocity and inclination angle, their linear stability depends only on the first derivative of the used disjoining pressure as for film rupture on a horizontal substrate [43], but not on the dynamics of the flow.

Numerical continuation techniques were used to calculate families of one-dimensional finite amplitude stationary solutions. Depending on mean film thickness different types of solution families were found and their linear stability was analyzed leading to the identification of linearly stable solutions and linearly unstable nucleation solutions. The solution families found for small inclination angle correspond to the family types found without inclination [43]. However, here the solutions are asymmetric and slide down the inclined plane with a velocity depending on period and mean film thickness. This motion has clearly no counterpart in the non-inclined case. Beside the families that have a counterpart in the case $\alpha = 0$ there exist stationary non-linear surface waves that are specific for $\alpha \neq 0$. They do only exist if both, molecular interaction and viscous flow driven by gravitation are present and depend

strongly on the ratio of mean film thickness and length scale of the diffuse interface.

The study of the solutions as a function of the period showed the existence of universal flat drop solutions whose velocity and plateau thicknesses are independent of period and mean film thickness. They have the form of flat or pancake drops of different length with a capillary ridge at their downstream end. The dependence of the properties of the non-universal and universal flat drops on period, inclination angle and interaction parameters was determined for both, relatively large but unrealistic and very small ratios of gravitation and molecular interaction. The influence of the parameter a describing the wetting properties was also determined.

Studying the flat drops we have found that with increasing inclination angle the upper (lower) plateau thickness decreases (increases), the velocity increases, and the receding dynamic contact angle decreases. For relatively large G the advancing dynamic contact angle shows a non-monotonic behavior as a function of the velocity, it increases first then decreases even below its static equilibrium value [44]. For very small G we studied the transition between non-universal and flat drops when increasing the inclination angle and found in the flat drop regime a monotonic decrease of the advancing contact angle with increasing velocity.

The universal regime breaks down if one of the plateau thicknesses approaches the mean film thickness. The study of the non-universal families has revealed an hysteresis effect, when jumps between a small and a large amplitude solution occur that both exist for a certain range of inclination angles for some mean film thicknesses. The existence of the branch of stable small amplitude solutions may in an experiment lead to the impression of stable flat film flow in the linearly unstable mean thickness range, because no large amplitude solutions can be seen without overcoming a nucleation solution. The occurring surface wave may go unnoticed because of their very small amplitude.

A first outlook towards two-dimensional calculations showed the transition from oval stationary drops, to stationary drops with a cusp at its back, and further to drops that periodically pinch off small satellite drops at the cusp. This three types of drops are exactly the ones found recently in an experiment [40]. In the study of the stability of fronts we have found both, transversal instabilities of advancing *and* receding fronts. To our knowledge, this is the first report on receding fronts found in theoretical models for the movement of liquid fronts. The findings may be applicable to instabilities found for receding fronts in dewetting [50,51].

Most work done on liquid sheets or ridges flowing down an inclined plane [28,35,52] takes a totally different approach than we have taken here. Based on the fact that they study situations that are a superposition of spreading and sliding going on forever, they analyze separately the three regions: (1) upstream end; (2) central part; and (3) downstream end of the ridge and scale them differently in time assuming respective power-law

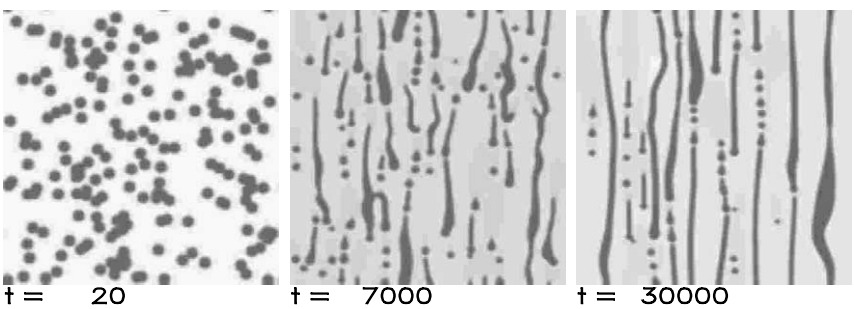

Fig. 18. The same as Fig. 17 but for a larger domain and 200 initial drops. After a long time, rivulets are formed streaming downwards. 512×512 points for a domain size of 1900.

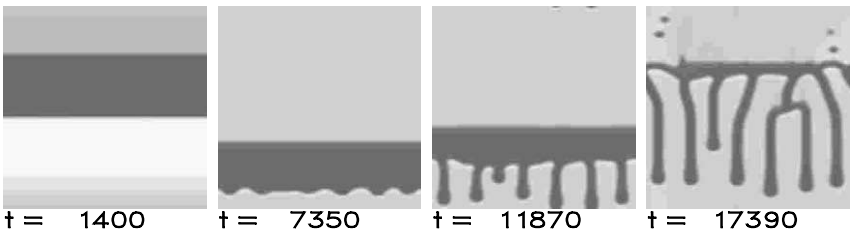

Fig. 19. Falling film, where the initial condition is a liquid ridge as explained in the main text. The advancing front gets unstable to a periodic transverse instability and fingering can be observed. 256×256 points. $G = 0.2$, $\alpha = 0.1$, $a = 0.2$ and domain size 950.

dependence. Then they determine similarity solutions in the regions (1), (2) and (3) and match them together. An additional problem of most models in the literature is that in slip models the dynamic contact angle is explicitly fixed at the contact line [31,36] or varies in a prescribed way with velocity [35]. In a precursor film model, however, the contact angle is zero without motion although with motion a mesoscale dynamic contact angle depends on the imposed velocity.

On the contrary, here we do not study the superposition of spreading and sliding, but the movement of sliding drops of constant shape in a moving frame as observed by Podgorski [40]. When the inclination angle vanishes, the shape of our droplets converges to the equilibrium shape of a drop of a partially wetting liquid on a horizontal plane. All the ad-hoc parameters in the above approach (static and dynamic contact angle, drop velocity, drop and precursor film thickness) are deduced within our theory from the two parameters describing wetting properties and ratio of gravitation to molecular interaction. If the liquid volume in an individual drop is small, also the volume influences the drop properties.

Because the rupture of a thin film on a horizontal substrate due to molecular interactions is closely related to the decomposition of a binary mixture as described by the Cahn–Hilliard equation [53,9,43], the sliding drops treated here have a close relationship to moving concentration profiles in a convective Cahn–Hilliard model [45]. The convective Cahn–Hilliard equation can be seen as a special case of our film evolution Eq. (6). Taking ε and g to be small deviations defined by $h(x) = h_c + \varepsilon(x)$ and $G = G_c + g$, close to the critical point ($G_c = 1/4$, $h_c = \ln 4$) (see Section 3) ($\partial_h f$ can be expressed as a cubic [43] and Eq. (6) writes

$$\partial_t \varepsilon = -\partial_x \Big\{ (h_c - \ln a + \varepsilon)^3 \times \Big[\partial_x (\partial_{xx}\varepsilon - \frac{f_4}{6}\varepsilon^3 - g\varepsilon) + \alpha g \Big] \Big\}, \tag{23}$$

where f_4 is short for $\partial_{hhhh} f|_{h_c}$. Assuming $\varepsilon \ll 1$, $g = O(\varepsilon)$, $f_4 = O(\varepsilon^{-1})$, $x = O(\varepsilon^{-1/2})$, $\alpha = O(\varepsilon^{-1/2})$ and $t = O(\varepsilon^{-2})$, in lowest order of ε Eq. (23) takes the form:

$$\partial_t \varepsilon = -\partial_{xx}\Big[\partial_{xx}\varepsilon - \frac{f_4}{6}\varepsilon^3 - g\varepsilon \Big] + \frac{6\alpha g}{h_c^2}\varepsilon\partial_x\varepsilon. \tag{24}$$

Another scaling of t, x and h transforms this equation into,

$$\partial_t \varepsilon = -\partial_{xx}[\partial_{xx}\varepsilon - \varepsilon^3 - \varepsilon] + \chi\varepsilon\partial_x\varepsilon, \tag{25}$$

with χ the only remaining parameter. This is the convective Cahn–Hilliard equation studied in [45] and itself related to the Kuramoto–Sivashinsky equation used to describe formation of small amplitude structures on falling liquid films [1]. This analogy has some consequences that should be further exploited in the future. So it can be expected that something similar to the dynamical wetting transition with hysteresis described in Ref. [44], i.e. the existence of both, linearly stable small *and* large amplitude concentration profiles for identical driving χ, can be found in the convective Cahn–Hilliard model. Also the results for the convective Cahn–Hilliard model [45] on the crossover between concentration profiles unstable and stable to coarsening lead to the hypothesis of an analogue to this transition for drop profiles on an inclined plane at least for certain values of mean film thickness and inclination angle.

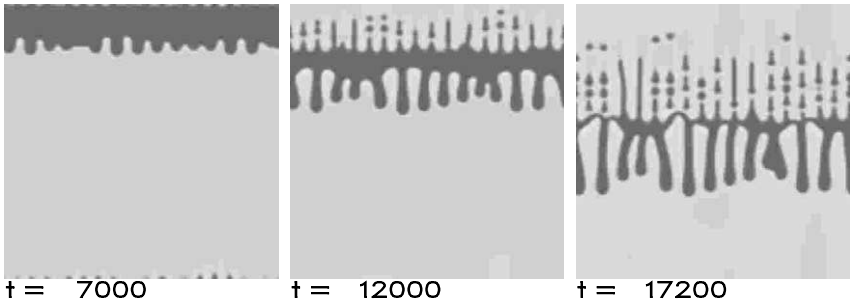

Fig. 20. The same as Fig. 19 but for a larger geometry and smaller angle α. Also the trailing edge of the wall is now unstable. 512×512 points, $\alpha = 0.1$ and domain size 1900.

Acknowledgements

This research was supported by the European Union under ICOPAC grant HPRN-CT-2000-00136, by the German Academic Exchange Board (DAAD) under grant D/98/14745, by the Deutsche Forschungsgemeinschaft under grant TH781/1-1 and by the Spanish Ministry of Education and Culture under grant PB 96-599. We would like to thank U. Bahr, G. Diener, E. Knobloch, L. Pismen and V. Starov for helpful discussions.

References

[1] A. Oron, S.H. Davis, S.G. Bankoff, Rev. Mod. Phys. 69 (1997) 931.
[2] P. de Gennes, Rev. Mod. Phys. 57 (1985) 827.
[3] B.V. Derjaguin, Zh. Fiz. Khim. 14 (1940) 137.
[4] B.V. Derjaguin, N.V. Churaev, V.M. Muller, Surface Forces, Consultants Bureau, New York, 1987.
[5] G.E. Teletzke, H.T. Davis, L.E. Scriven, Rev. Phys. Appl. 23 (1988) 989.
[6] R.J. Hunter, Foundation of Colloid Science, vol. 1, Clarendon Press, Oxford, 1992.
[7] J.N. Israelachvili, Intermolecular and Surface Forces, Academic Press, London, 1992.
[8] V.M. Starov, Adv. Colloid Interface Sci. 39 (1992) 147.
[9] V.S. Mitlin, J. Colloid Interface Sci. 156 (1993) 491.
[10] H.S. Kheshgi, L.E. Scriven, Chem. Eng. Sci. 46 (1991) 519.
[11] G. Reiter, Phys. Rev. Lett. 68 (1992) 75.
[12] U. Thiele, K. Neuffer, Y. Pomeau, M.G. Velarde, Colloids Surf. A: Physicochem. Eng. Aspects, 206 (2002) 135–155.
[13] A.M. Cazabat, Cont. Phys. 28 (1987) 347.
[14] L. Hocking, Phys. Fluids 6 (1994) 3224.
[15] H. Greenspan, J. Fluid Mech. 84 (1978) 125.
[16] V.E.B. Dussan, Ann. Rev. Fluid Mech. 11 (1979) 371.
[17] P. Kapitza, S. Kapitza, Zh. Exp. Teor. Fiz. 19 (1949) 105.
[18] J. Liu, J. Gollub, Phys. Fluids 6 (1994) 1702.
[19] T.B. Benjamin, J. Fluid Mech. 2 (1957) 554.
[20] C. Yih, Phys. Fluids 6 (1963) 321.
[21] D. Benney, J. Math. Phys. 45 (1966) 150.
[22] B. Gjevik, Phys. Fluids 13 (1918) 1970.
[23] S. Lin, J. Fluid Mech. 63 (1974) 417.
[24] H.-C. Chang, Phys. Fluids A 1 (1989) 1314.
[25] H.-C. Chang, Annu. Rev. Fluid Mech. 26 (1994) 103.
[26] S. Joo, S. Davis, S. Bankoff, J. Fluid Mech. 230 (1991) 117.
[27] H.-C. Chang, E. Demekhin, E. Kalaidin, J. Fluid Mech. 294 (1995) 123.
[28] H.E. Huppert, Nature 300 (1982) 427.
[29] N. Silvi, V.E.B. Dussan, Phys. Fluids 28 (1985) 5.
[30] L. Hocking, J. Fluid Mech. 79 (1977) 209.
[31] N. Spaid, G. Homsy, Phys. Fluids 8 (1996) 460.
[32] L.W. Schwarz, Phys. Fluids A 1 (1989) 3.
[33] L. Hocking, M. Miksis, J. Fluid Mech. 247 (1993) 157.
[34] D.E. Kataoka, S.M. Troian, J. Colloid Interface Sci. 192 (1997) 350.
[35] L. Hocking, J. Fluid Mech. 211 (1990) 373.
[36] D. Moyle, M.-S. Chen, G. Homsy, Int. J. Multiphase Flow 25 (1999) 1243.
[37] Y.D. Shikhmurzaev, J. Fluid Mech. 334 (1997) 211.
[38] L. Mahadevan, Y. Pomeau, Phys. Fluids 11 (1999) 2449.
[39] D. Richard, D. Quere, Europhys. Lett. 48 (1999) 286.
[40] T. Podgorski, J.-M. Flessellas, L. Limat Phys. Rev-Lett. 87, 036102. (2001).
[41] D.M. Anderson, G.B. McFadden, A.A. Wheeler, Annu. Rev. Fluid Mech. 30 (1998) 139.
[42] L.M. Pismen, Y. Pomeau, Phys. Rev. E 62 (2000) 2480.
[43] U. Thiele, M.G. Velarde, K. Neuffer, Y. Pomeau, Phys. Rev. E 64, 031602 (2001).
[44] U. Thiele, M.G. Velarde, K. Neuffe, M. Bestehoin, Y. Pomeau, Phys. Rev. E 64, 061601 (2001).
[45] A. Golovin, A. Nepomnyashchy, S. Davis, M. Zaks, Phys. Rev. Lett. 86 (2001) 1550.

[46] L. Nguyen, V. Balakotaiah, Phys. Fluids 12 (2000) 2236.
[47] E. Doedel, A. Champneys, T. Fairfrieve, Y. Kuznetsov, B. Sandstede, X. Wang, AUT097: Continuation and bifurcation software for ordinary differential equations, Concordia University, Montreal, 1997.
[48] M.F.G. Johnson, R.A. Schluter, M.J. Miksis, S.G. Bankoff, J. Fluid Mech. 394 (1999) 339.
[49] J.A. Diez, L. Kondic, Phys. Rev. Lett. 86 (2001) 632.
[50] A. Sharma, G. Reiter, J. Colloid Interface Sci. 178 (1996) 383.
[51] K. Jacobs, Stabilität and Dynamik ftüssiger Polymerfilme, PhD-thesis, ISBN 3-930803-10-0, 1997.
[52] S. Troian, E. Herbolzheimer, S. Safran, J. Joanny, Europhys. Lett. 10 (1989) 25.
[53] J.W. Cahn, J.W. Hillard, J. Chem. Phys. 28 (1958) 258.